DESIGN AND DEVELOPMENT OF A LOW-COST SOFT-ROBOTIC ACTUATOR SYSTEM FOR HAND REHABILITATION: THE E-GLOVE PROTOTYPE

Aldo Dwi Putra Pasaribu¹, Wahyu Dwi Lestari^{1*}

¹ Department of Mechanical Engineering, Faculty of Engineering, University of Pembangunan Nasional Veteran Jawa Timur

Abstract

Stroke and traumatic brain injury often lead to hand motor impairments that limit independence and quality of life. This study presents a portable, low-cost actuator system for the E-Glove: a soft robotic glove designed to deliver continuous passive motion (CPM) for hand rehabilitation. The actuator design was envisioned to be capable of producing sufficient torque to overcome severe stiffness (resistive force ≥8 N), user-friendly control, and portability. The actuator module consists of two TowerPro MG996R servo motors controlled by an Arduino Nano, with capacitive touch sensors allowing three discrete speed settings (35.7, 45.5, and 50.0 degrees/s) and RGB LED feedback. Biomechanical analysis determined a lever arm of 0.07 m and calculated a maximum resistive torque of 12.28 N-m, resulting in a safety factor >1 for severe flexure. Prototype testing confirmed reliable operation at all speed levels and safe disengagement upon power-off. The detachable actuator housing, powered via USB-C, supports home-based therapy and remote monitoring. This work addresses critical barriers to accessibility, promoting high-frequency rehabilitation outside clinical settings.

Keyword: Soft robotic glove; hand rehabilitation; continuous passive motion; servo actuator; post-stroke therapy

INTRODUCTION

The human hand is one of the most complex structures in the body, serving as the primary manipulator for environmental interaction. Skeletal Structure: The skeletal framework of the hand consists of 27 bones with eight carpals forming the wrist, five metacarpals forming the palm, and fourteen phalanges within the fingers. This skeleton is not rigid, but rather forms a series of longitudinal and transverse curves that allow the hand to conform to different shapes of objects. The second and third metacarpals serve as stable central pillars, while the fourth and fifth metacarpals exhibit greater mobility, allowing a "cupping" motion for firm grasping (Stefano, 2023).

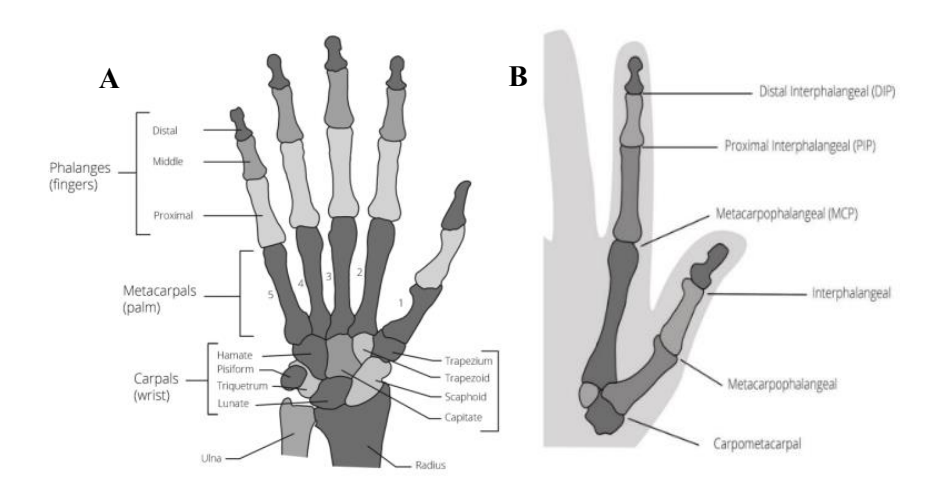


Figure 1. (A) Skeletal Structure of the Human Hand. (B) Anatomy of the Human Hand Joint.

Hand movement is facilitated by a series of synovial joints, technically referred to as articulations. These articulations include the Metacarpophalangeal (MCP) joint, which is a condyloid joint that allows movement in two planes, namely flexion-extension and abduction-adduction.

Furthermore, the Proximal Interphalangeal (PIP) and Distal Interphalangeal (DIP) joints are ginglymus (hinge) joints, which exclusively allow uniplanar motion, specifically flexion-extension. (Duruöz, 2019; Stefano, 2023). Understanding the degrees of freedom (DoF) and normative Range of Motion (ROM) for each of these articulations is essential for programming the kinematics of the actuator, to ensure operational effectiveness and user safety.

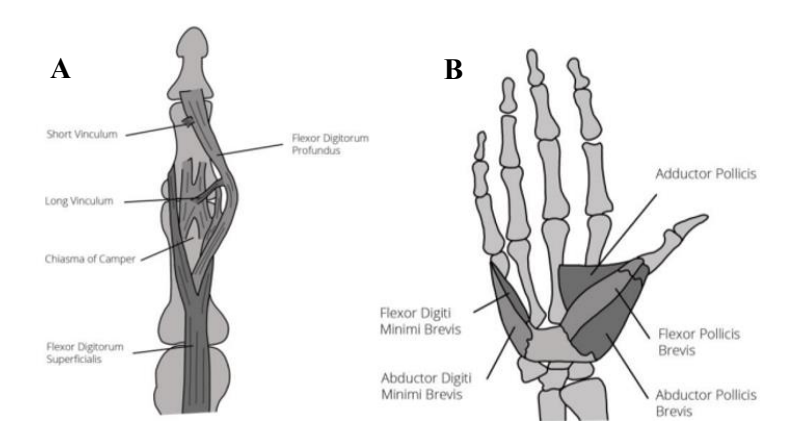


Figure 2. (A) Musculature of the Human Finger. (B) Musculature of the Human Palm.

Beyond the articulations, digital motion is governed by two principal muscle groups: the extrinsic and intrinsic muscles. The extrinsic muscles originate in the forearm, with their corresponding tendons extending distally into the hand. These muscles are primarily responsible for gross motor functions and the generation of grip force. For digital flexion (i.e., forming a fist), the primary actuators are the Flexor Digitorum Superficialis (FDS), which flexes the MCP and PIP joints, and the Flexor Digitorum Profundus (FDP), which effects flexion across all three digital joints (MCP, PIP, and DIP) (Saeedi-Boroujeni et al., 2023). Conversely, digital extension (i.e., opening the hand) is principally mediated by the Extensor Digitorum Communis (EDC) muscle. In contrast, the intrinsic muscles are located entirely within the confines of the hand, encompassing muscles such as the lumbricals and the interossei. These muscles are integral to fine motor control and intricate digital coordination. A robotic glove that administers passive motion will consequently stretch both muscle groups, thereby aiding in the prevention of muscular contractures and the preservation of tissue elasticity (Huang et al., 2024).

Motor dysfunction after neurological injury is not simply a matter of muscle deficits, but rather stems from disturbances in the neural control system. Intentional hand movements, from the cerebral motor cortex, with neural signals that are then transmitted through the corticospinal tract (CST) which is the main neural pathway to motor neurons in the spinal cord, which ultimately innervate the muscles of the hand. In the event of a stroke or brain injury, lesions affecting the motor cortex or CST can disrupt this command pathway, leading to paralysis (loss of motor function) or paresis (muscle weakness) (Chen et al., 2020).

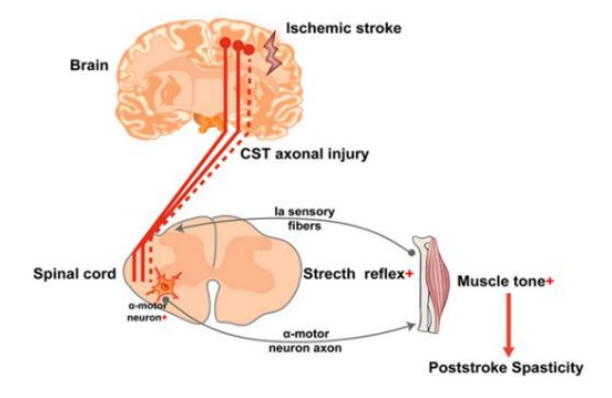


Figure 3. Diagram Illustrating the Pathophysiology of Paresis Following CST Injury

Pathophysiology, and clinical manifestations neurological insults, such as ischemic or hemorrhagic stroke and traumatic brain injury, frequently result in lesions to the motor cortex and efferent (motor) pathways, such as the corticospinal tract. The consequences of this damage on the upper extremities, particularly the hand, are profoundly debilitating and significantly impact independence in Activities of Daily Living (ADLs)(Kruse et al., 2020). The primary clinical manifestations of this impairment include:

- Hemiparesis or Hemiplegia: Weakness (paresis) or complete paralysis (plegia) on the contralateral side of the body relative to the cerebral lesion. This results in an inability to volitionally initiate digital flexion and extension (Duruöz, 2019).
- Spasticity: One of the most common complications, defined as a velocity-dependent increase in muscle tone in response to stretch (an exaggerated stretch reflex). In the hand, it often manifests as a dominant flexion pattern, wherein the digits and wrist tend to assume an involuntary flexed posture and resist passive extension (Huang et al., 2024).
- Joint Contracture: If the spastic hand is not mobilized regularly, the muscles, tendons, and ligaments undergo adaptive shortening. Connective tissues surrounding the joint also become stiff, ultimately leading to a permanent loss of Range of Motion (ROM). This condition, known as a contracture, is exceedingly difficult to resolve once established (Bates & Sunderam, 2023).
- Learned Non-Use: Resulting from the difficulty in using the affected hand, the patient subconsciously begins to neglect it and develop an over-reliance on the unimpaired limb. This behavioral phenomenon can exacerbate muscle atrophy and further diminish the cortical representation of the affected hand (Yurkewich et al., 2020).

The repetitive passive motion generated by the E-GLOVE operates via two primary mechanisms: the prevention of mechanical complications and, more critically, the facilitation of neurological recovery. Continuous Passive Motion (CPM) at its most fundamental level, this prototype is expected to feature a Continuous Passive Motion (CPM) therapeutic modality, wherein the joints are mechanically moved through a predetermined ROM without requiring muscular effort from the patient. The mechanical benefits of CPM are well-established, particularly in the early phase of recovery (Yasuda et al., 2025). Regular mobilization prevents the formation of soft-tissue adhesions, combats the development of contractures by maintaining musculotendinous length, enhances synovial fluid circulation for cartilage nutrition, and assists in the reduction of edema (swelling) (Wu et al., 2021). The Paradox of Passive Motion and Active Neurological Stimulation: The most impactful mechanism of this therapy occurs at the neurological level. A phenomenon that can be termed the "paradox of passive motion" exists: a motion that is mechanically passive for the body can trigger highly active information processing and reorganization within the brain (Mansour et al., 2022).

The repetitive passive motion generated by the actuator system is expected to operate through two main mechanisms, namely preventing mechanical complications and facilitating neurological recovery. Continuous Passive Motion (CPM) at its most basic level, is expected to perform a therapeutic modality where the joint is mechanically moved through a predetermined ROM without requiring muscular effort from the patient. In several studies, the mechanical benefits of CPM have been well proven, especially in the early phases of recovery (Wang et al., 2023). Regular mobilization prevents the formation of soft tissue adhesions, combats the development of contractures by maintaining musculotendinous length, improves synovial fluid circulation for cartilage nutrition, and helps reduce edema (swelling). The most impactful mechanism of this therapy occurs at the neurological level. A phenomenon that can be referred to as the "passive movement paradox", where movements that are mechanically passive for the body, can trigger highly active information processing and reorganization within the brain (Abd Elhady et al., 2025).

MATERIALS AND METHODS

The design methodology applied is holistic, integrates user needs and is more economical from the beginning of the project. The approach is taken so that every design decision, from component selection to software design, has a strong justification and contributes to the ultimate goal of the

project. A diagram illustrating the design methodology and operational principles for the fabrication of the E-Glove actuator system is in figure 4.

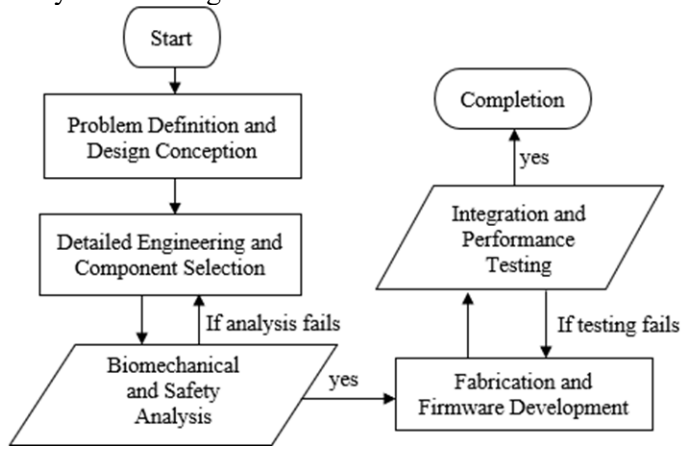


Figure 4. Flowchart of the Design Methodology and Operating

Design Requirements and Biomechanical Analysis

The torque required to move the finger structure is the product of the resistive force and the length of the lever arm. Resistive forces can arise from spasticity. Spasticity is a complex and variable phenomenon. Studies using quantitative biomechanical methods to measure resistance to passive stretch in the hands of stroke survivors have identified significant nerve (spasticity) (Hwang et al., 2021; Pan et al., 2021).

Although specific research on spasticity values for joints in the finger structure of the human hand does not exist, for the purpose of this design, spasticity values for the wrist. In the journal "Quantitative Assessment of Hand Spasticity After Stroke: Imaging Correlates and Impact on Motor Recovery", the prevalence of post-stroke spasticity was found to increase over time. At 3 weeks (T1), 33% of patients showed spasticity, an occurrence that increased to 51% at 6 months (T3). Figure 5 categorizes post-stroke patients from no spasticity (<3.4 N), moderate spasticity (between 3.4 N and 8 N), and severe spasticity (>8 N) (Bates & Sunderam, 2023).

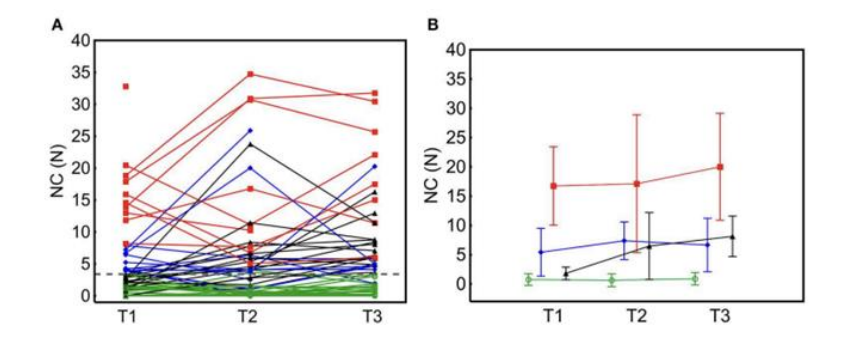


Figure 5. (A) Spasticity Trajectories for Individual Subjects, (B) Mean Spasticity Levels at Sequential Time Points

(T1 = 3 weeks post-insult; T2 = 3 months post-insult; T3 = 6 months post-insult)

Referring to the study "Dimensions of the Proximal Interphalangeal Joint for Surface Replacement Prosthesis Design," the effective lever arm is defined as the distance from the joint's center of rotation (i.e., the metacarpophalangeal joint, MCP) to the point of force application by the actuator binder. For flexion or grasping movements, this distance is roughly equivalent to the combined length of the proximal and middle phalanges. Anthropometric data shows that the length of the proximal phalanges can range from 29-52 mm, while the length of the middle phalanges ranges from 16-35 mm. Using representative average values, the total lever arm length can be estimated to be approximately 45 mm + 25 mm = 70 mm (0.07 m)(Saeedi-Boroujeni et al., 2023).

$$\tau \operatorname{res} = f_{spasticity} \times \operatorname{arm length} \tag{1}$$

$$FoS = \frac{\tau_{\text{servo motor}}}{\tau_{res}} \tag{2}$$

Hardware Architecture

This biomechatronic system is designed as an integrated, portable, and easy-to-use unit, consisting of hardware and software components that work synergistically. The hardware structure was chosen by balancing functionality, component availability and cost-effectiveness. The central control unit uses an ATmega328P-based Arduino Nano microcontroller board. This platform was chosen due to its compact size, low power consumption, sufficient I/O pins, and extensive community and library support, which speeds up the development process. For the sensors and user interface, two TTP223 capacitive touch sensor modules were used that serve as the power button and speed level control button of the actuator system. The first sensor functions as a toggle switch to power the system on and off. The second sensor is used to cycle through the operational speed levels. Touch sensors were selected for their ease of integration, requirement of no mechanical actuation force, and provision of a modern and intuitive interface.



Figure 6. (A) ATmega328P-based Arduino Nano, (B) TTP223 Capacitive Touch Sensor, (C) TowerPro MG996R Servo Motor

Visual Feedback: An RGB (Red, Green, Blue) LED is used to provide visual feedback to the user regarding the system's operational status (on/off) and the active speed level (Blue for Level 1, Green for Level 2, Red for Level 3). The system is powered via a USB Type-C connector, a strategic design choice to align with modern connector standards, ensuring ease of charging with ubiquitous mobile phone adapters or power banks.

Actuator system, use the frame to house the electronic components (Arduino, breadboard, sensors) - the so-called "controller box" - was made from cardboard, as depicted in Figure 7. This choice of material was limited to experimentation and will later be replaced with 3D printing. The aim was to quickly validate the core functionality and ergonomic layout at minimal cost. Cardboard allows for easy modifications-cutting new holes for wires, repositioning sensors, or adjusting circuit board placement-allowing design iterations to be done in minutes rather than hours or days. This approach intelligently focuses resources on validating critical functions first.

TowerPro MG996R servo motor was chosen for its dimensional compatibility with the design. Operating at 4.8V, this servo can produce a stall torque of 9 kg-cm, which is equivalent to 0.883 Nm. Therefore, analysis was required to determine whether the TowerPro MG996R had sufficient capability to overcome the resistive forces presented by patients with conditions up to and including high spasticity.

Firmware and Control Logic

This actuator system is controlled by an Arduino Nano, which processes input signals from two touch sensors to manage the system outputs. The first sensor serves as a power switch (on/off), while the second sensor allows the user to cycle through predefined speed settings. Based on these inputs, the Arduino commands two main outputs: a pair of 180° servo motors and an RGB LED. The servos execute the therapeutic motion at the selected speed, and the RGB LEDs provide intuitive visual feedback, indicating the system's power status and current speed level through different colors. The complete wiring scheme for this integrated assembly is detailed in Figure 7.



Figure 7. System Wiring and Component Integration

The control logic executed on the Arduino Nano is central to the functionality of the actuator system, with the code structurally designed to ensure reliable, responsive and safe operation. The main control structure uses simple state machine logic managed by a boolean variable, systemOn, which ensures that all motor and LED operations are executed only when the system is in the "on" state to prevent unwanted movement. To maintain readability and ease of operation, the code is organized into several mechanical key functions.

```
// --- VARIABEL STATUS DAN KONTROL ---
// Status utama sistem

bool sistemMenyala = false;
// Status level kecepatan dan warna
int levelOperasi = 1;
// Variabel untuk menyimpan nilai delay sesuai level kecepatan
int nilaiDelay = 28;

// Variabel untuk gerakan looping servo
int posisiServo = 0;
int arahGerak = 1;

// Variabel untuk deteksi sentuhan pada kedua sensor
int statusSentuh1 = 0;
int statusSentuh2 = 0;
int statusSentuh2 = 0;
int statusSentuh1erakhir1 = 0;
int statusSentuh1erakhir2 = 0;
```

Figure 8. Status And Control Variables

The setLedAndSpeed() function efficiently manages the RGB LED color and assigns the delayValue variable, which controls the servo motor speed. This variable is then utilized by executeLoopingMotion(), the core function that generates the therapeutic motion by incrementally changing the servo position from 0 to 180 degrees and back. Finally, to guarantee safety, the returnServosToHome() function slowly returns the servos to their 0-degree position when the system is powered down, preventing the user's digits from being locked in a flexed position.

```
// Kontrol OM/OFF dengan Sensor 1
if (statusSentuhl == HIGH && statusSentuhlTerakhir1 == LOW) {
    sistemMenyala = !sistemMenyala; // Toggle status

128
129
if (sistemMenyala) { // Jika sistem BARU SAJA dinyalakan
    levelOperasi = 1; // Selalu mulai dari Level 1
    posisiServo = 0; // Reset posisi servo
    arahGerak = 1;
    Senial.println("Sistem Dinyalakan! Memulai di Level 1.");
    } else { // Jika sistem BARU SAJA dinatikan
    Serial.println("Sistem Dinyalakan! Memulai di Level 1.");
    kembalikanServoKeawal();
    matikanLedRgb();
    Serial.println("Sistem Dimatikan! Mengembalikan servo...");
    kembalikanServoKeawal();
    matikanLedRgb();
    Serial.println("Sistem mati. Servo di posisi awal.");
    }

delay(50); // Debounce
```

Figure 9. On/Off Control Function of Sensor 1

Input management from the touch sensors is performed during each iteration of the loop(), where the implementation of software debouncing techniques is crucial. By applying a delay(50)

after a valid touch detection, this engineering practice effectively prevents erroneous multiple readings that could be caused by signal fluctuations or unstable contact. This ensures that each physical touch triggers only a single state change, such as toggling the system's power or advancing the operational level.

Furthermore, the code allows for quantitative kinematic validation. The angular velocity of the servo can be analyzed from the executeLoopingMotion() function, where the motor moves one degree per step, followed by a pause defined by delayValue in milliseconds. Based on this logic, the angular velocity (ω) can be accurately estimated using the corresponding formula below:

$$\omega \approx \frac{1 \text{ derdeg}}{\text{nil} \cdot \text{delayValue s}} \times \frac{1000 \text{ ms}}{1 \text{ s}} = \frac{1000}{\text{nil} \cdot \text{delayValue '}} A_{\text{o}} \text{ deg}$$
(3)

Based on the delayValue in the setLedAndSpeed() function:

- Level 1: delay Value = 28 ms $\rightarrow \omega \approx 28/1000 \approx 35.7$ deg/s (corresponds to the claim ~ 36 deg/s).
- Level 2: delayValue = 22 ms $\rightarrow \omega \approx 22/1000 \approx 45.5$ deg/s (corresponds to the claim~45 deg/s).
- Level 3: delayValue = 20 ms $\rightarrow \omega \approx 20/1000 = 50.0$ deg/s (corresponds to the claim ~ 51 deg/s).

```
// Fungsi untuk mengatur warna LED dan kecepatan sesuai level
void aturLedDanKecepatan() {
switch (levelOperasi) {
case 1: // Biru, 36 der/det
analogWrite(PIN_LED_G, 0);
analogWrite(PIN_LED_G, 0);
analogWrite(PIN_LED_B, 255);
nilaiDelay = 28;
break;
case 2: // Hijau, 45 der/det
analogWrite(PIN_LED_B, 0);
analogWrite(PIN_LED_B, 0);
analogWrite(PIN_LED_B, 0);
inilaiDelay = 22;
break;
case 3: // Merah, 51 der/det
analogWrite(PIN_LED_B, 0);
break;
break;
```

Figure 10. Speed Control and Corresponding Lamp Adjustment Function

The tendon actuation mechanism in this prototype is designed to mimic the fundamental motions of the hand through two primary phases. During the flexion phase (closing the hand), servo motor 1 retracts the cord, transmitting force to the fingertips. This force generates a moment (torque) at each digital joint—Distal Interphalangeal (DIP), Proximal Interphalangeal (PIP), and Metacarpophalangeal (MCP)—causing simultaneous flexion. Therapeutically, this motion passively stretches the extrinsic and intrinsic extensor muscles (e.g., Extensor Digitorum Communis), which is critical for maintaining their flexibility. Conversely, during the extension phase (opening the hand), servo motor 2 moves in the opposite direction, releasing tension on its cord and allowing servo 1 to pull the digits back into an extended position. This movement is crucial as it directly counteracts the dominant flexor spasticity pattern and provides a controlled stretch to the powerful flexor muscles, such as the Flexor Digitorum Profundus and Superficialis.

Performance Testing

The system is activated by pressing touch sensor 1. Upon activation, the RGB LED immediately illuminates in blue, and the two servo motors begin their therapeutic motion cycle. They rotate from their initial position (0°) to their final position (180°) and then immediately return to 0° . This process repeats in a continuous loop, driving the E-Glove's constant flexion (grasping) and extension (opening) action. The user can cycle through three distinct speed levels using touch sensor 2. The system starts at Level 1 by default.

- Level 1: Indicated by a blue LED. The servos operate at 35.7 deg/s.
- Level 2: Indicated by a green LED. The servos operate at 45.5 deg/s.
- Level 3: Indicated by a red LED. The servos operate at 50.0 deg/s.

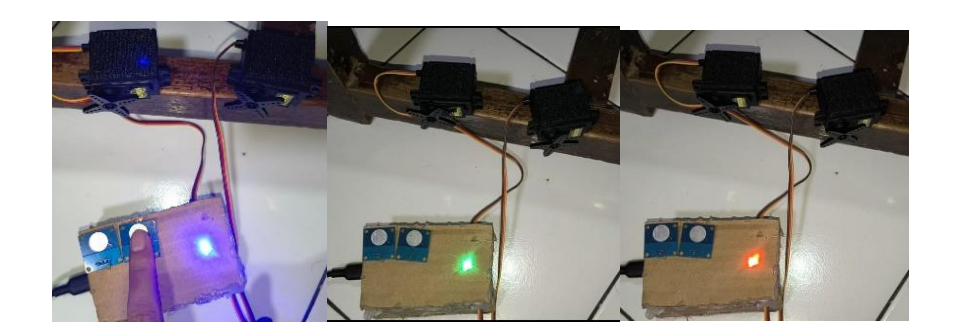


Figure 11. Intergation and Performance Testing Actuator System

Pressing sensor 2 at Level 3 will loop the system back to Level 1, allowing for easy and continuous speed adjustment. A key design feature is the seamless speed transition. When the user changes the speed level mid-cycle, the servo motors continue their movement from their current position without resetting or stopping. This ensures the user experience is smooth, comfortable, and feels safe throughout the therapy session.

RESULTS AND DISCUSSION

Mechanical and Ergonomic Performance

The Factor of Safety (FoS) is determined by comparing the available torque from the actuator to the required torque to overcome resistance. The resulting FoS value dictates the adequacy of the servo motor in overcoming the resistive forces generated by spastic hand musculature. The target design criterion is an FoS greater than 1 (FoS > 1), even for patients exhibiting high spasticity (resistive force > 8 N).

Consequently, an analysis was necessary to determine if the TowerPro MG996R servo is capable of overcoming the resistance presented by patients with conditions up to and including severe spasticity. By applying the relevant equations and evaluating the resulting FoS of the motor across the full spectrum of spasticity values (from minimum to maximum documented in the literature), the graph presented in Figure 7 was generated.

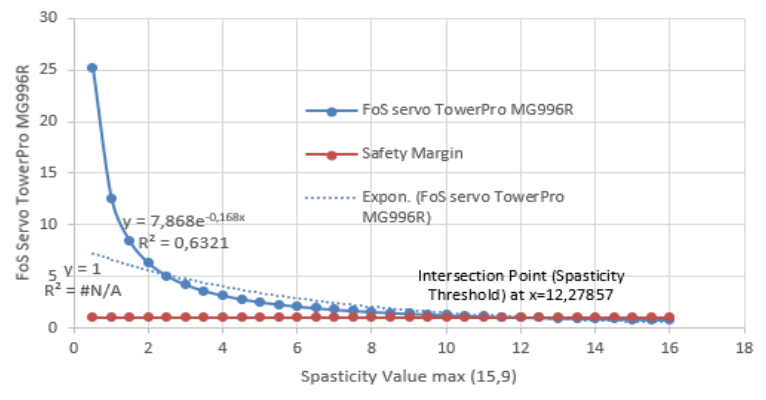


Figure 12. Plot of the Factor of Safety (FoS) as a Function of Spasticity Level in a Post-Stroke Cohort

Based on Figure 7, it can be concluded that the Tower Pro MG996R servo motor is capable of overcoming the resistance from severe spasticity in post-stroke patients (forces > 8 N) up to a calculated limit of 12.27857 N. Therefore, given its compatibility and sufficient torque, the Tower Pro MG996R servo motor is deemed suitable for use in the fabrication of this prototype.

Based on Figure 5, it can be concluded that the Tower Pro MG996R servo motor is capable of overcoming the resistance from severe spasticity in post-stroke patients (forces > 8 N) up to a calculated limit of 12.27857 N. Therefore, given its compatibility and sufficient torque, the Tower Pro MG996R servo motor is deemed suitable for use in the fabrication of this prototype.

Therapeutic Implications

The project began by investigating the real-world challenges faced by post-stroke survivors, guided by a comprehensive review of existing literature. This foundational research allowed for the identification of key patient requirements, which formed the conceptual basis for the E-Glove's actuator system. To ensure the concept's viability, critical consideration was given to motor impairments, specifically the functional resistance caused by spasticity. It was therefore imperative to confirm that the proposed system could overcome this resistance. This validation was achieved through kinematic estimations, torque validation, and a Factor of Safety (FoS) analysis. Following this analysis, component compatibility and overall user comfort were prioritized as key design drivers.

The physical assembly and programming phase commenced only after all selected components successfully passed the biomechatronic analysis. The components were then assembled according to the specified system design. The Arduino firmware was developed with a primary focus on user safety, comfort, and core therapeutic functionality.

Limitations and Future Work

A primary limitation is the fabrication of the controller housing from cardboard. While this material was advantageous for rapid prototyping and iterative design at a low cost, it lacks the durability, aesthetic finish, and protective qualities required for a clinical or home-use medical device. Future work will prioritize the design and fabrication of a robust, professional-grade enclosure using 3D printing or injection molding. This will not only improve the device's longevity and user appeal but also ensure better protection for the internal electronic components.

Finally, while the dual-servo design is cost-effective and lightweight, future research could explore alternative actuation mechanisms that might offer quieter operation or more nuanced force control. This could involve investigating technologies like pneumatic actuators or shape memory alloys to further optimize the trade-off between performance, cost, and portability. Building upon the successful validation of this prototype, these future steps will be crucial in transitioning the E-Glove from a functional proof-of-concept to a market-ready therapeutic device.

CONCLUSION

Based on its design analysis, the actuator system is confirmed to be suitable for integration into the planned E-Glove, as it's capable of overcoming high spasticity by handling resistive forces up to 12.2 N. The design incorporates several key features for effective, real-world use, including three adjustable speed levels to tailor therapy to patient needs and a compact, USB Type-C powered design for full portability. As supported by the theoretical framework, the system's repetitive motion is also expected to have a significant impact on neuromuscular activation.

This combination of a cost-effective and portable design should substantially reduce the final manufacturing cost of the E-Glove. This ultimately enables patients to use the device directly at home, facilitating more frequent therapy sessions that can be monitored remotely and reducing the need for constant visits to healthcare facilities.

REFERENCES

- Abd Elhady, A. E. S., Ahmed, G. M., Hassan, A., Mohamed Ibrahim, S., & Mohamed Abdelmageed, S. (2025). Efficacy of robotic training gloves in improving hand function and movement in stroke patients. *Sport TK*, *14*, 1–17. https://doi.org/10.6018/sportk.660321
- Bates, M., & Sunderam, S. (2023). Hand-worn devices for assessment and rehabilitation of motor function and their potential use in BCI protocols: a review. *Frontiers in Human Neuroscience*, 17. https://doi.org/10.3389/fnhum.2023.1121481
- Chen, S., Li, Y., Shu, X., Wang, C., Wang, H., Ding, L., & Jia, J. (2020). Electroencephalography Mu Rhythm Changes and Decreased Spasticity After Repetitive Peripheral Magnetic Stimulation in Patients Following Stroke. *Frontiers in Neurology*, 11(September), 1–12. https://doi.org/10.3389/fneur.2020.546599
- Duruöz, M. T. (2019). Hand Function: A Practical Guide to Assessment, Second Edition. Hand Function: A Practical Guide to Assessment, Second Edition, March 2022, 1–357.

- https://doi.org/10.1007/978-3-030-17000-4
- Huang, L., Yi, L., Huang, H., Zhan, S., Chen, R., & Yue, Z. (2024). Corticospinal tract: a new hope for the treatment of post-stroke spasticity. *Acta Neurologica Belgica*, 124(1), 25–36. https://doi.org/10.1007/s13760-023-02377-w
- Hwang, D., Shin, J. H., & Kwon, S. (2021). Kinematic assessment to measure change in impairment during active and active-assisted type of robotic rehabilitation for patients with stroke. *Sensors*, 21(21). https://doi.org/10.3390/s21217055
- Kruse, A., Suica, Z., Taeymans, J., & Schuster-Amft, C. (2020). Effect of brain-computer interface training based on non-invasive electroencephalography using motor imagery on functional recovery after stroke a systematic review and meta-analysis. *BMC Neurology*, 20(1), 1–14. https://doi.org/10.1186/s12883-020-01960-5
- Mansour, S., Ang, K. K., Nair, K. P. S., Phua, K. S., & Arvaneh, M. (2022). Efficacy of Brain—Computer Interface and the Impact of Its Design Characteristics on Poststroke Upper-limb Rehabilitation: A Systematic Review and Meta-analysis of Randomized Controlled Trials. *Clinical EEG and Neuroscience*, 53(1), 79–90. https://doi.org/10.1177/15500594211009065
- Pan, B., Huang, Z., Jin, T., Wu, J., Zhang, Z., & Shen, Y. (2021). Motor function assessment of upper limb in stroke patients. *Journal of Healthcare Engineering*, 2021. https://doi.org/10.1155/2021/6621950
- Saeedi-Boroujeni, A., Purrahman, D., Shojaeian, A., Poniatowski, Ł. A., Rafiee, F., & Mahmoudian-Sani, M. R. (2023). Progranulin (PGRN) as a regulator of inflammation and a critical factor in the immunopathogenesis of cardiovascular diseases. *Journal of Inflammation (United Kingdom)*, 20(1), 1–14. https://doi.org/10.1186/s12950-023-00327-0
- Stefano, A. (2023). *The Fascinating Functional Anatomy of the Human Hand*. 07, 2–3. https://doi.org/10.37421/2684-4265.2023.7.275
- Wang, T., Liu, Z., Gu, J., Tan, J., & Hu, T. (2023). Effectiveness of soft robotic glove versus repetitive transcranial magnetic stimulation in post-stroke patients with severe upper limb dysfunction: A randomised controlled trial. *Frontiers in Neurology*, 13. https://doi.org/10.3389/fneur.2022.887205
- Wu, J., Cheng, H., Zhang, J., Yang, S., & Cai, S. (2021). Robot-Assisted Therapy for Upper Extremity Motor Impairment after Stroke: A Systematic Review and Meta-Analysis. *Physical Therapy*, 101(4), 1–13. https://doi.org/10.1093/ptj/pzab010
- Yasuda, H., Ueda, M., Ueno, K., Naito, Y., Ishii, R., & Takebayashi, T. (2025). Enhancing mu-ERD through combined robotic assistance and motor imagery: a novel approach for upper limb rehabilitation. *Frontiers in Human Neuroscience*, 19(June), 1–8. https://doi.org/10.3389/fnhum.2025.1571386
- Yurkewich, A., Kozak, I. J., Ivanovic, A., Rossos, D., Wang, R. H., Hebert, D., & Mihailidis, A. (2020). Myoelectric untethered robotic glove enhances hand function and performance on daily living tasks after stroke. *Journal of Rehabilitation and Assistive Technologies Engineering*, 7. https://doi.org/10.1177/2055668320964050